N72-25368

IDENTIFICATION OF ATMOSPHERIC STRUCTURE BY COHERENT MICROWAVE SOUNDING

William P. Birkemeier

University of Wisconsin

ABSTRACT

Two atmospheric probing experiments involving beyond-the-horizon propagation of microwave signals are reported. In the first experiment, Doppler-shift caused by the cross-path wind is measured by a phase-lock receiver with the common volume displaced in azimuth from the great-circle. Variations in the measured Doppler shift values are explained in terms of variations in atmospheric structure. The second experiment makes use of the pseudorandom sounding signal used in a RAKE communication system. Both multipath delay and doppler shift are provided by the receiver permitting the cross section of the layer structure of the atmosphere to be deduced. The angular dependance and the cross-path wind in each layer are displayed.

1. INTRODUCTION

This paper is concerned with the problem of identifying the structure and dynamics of the atmosphere from the coherent detection and analysis of sounding signals after their transmission through the scatter medium. Section I discusses the coherent CW soundings performed on the UW-Collins 230 km link. This work, which relies on the antenna beams for spatial resolution, has successfully identified cross-path winds in scattering strata at different heights and has led to a model which hopefully improves the understanding of the role of cross-path winds and atmospheric layer structure in the propagation mechanism. A model is presented which predicts the doppler shift of the

received signals in terms of the cross-path motion of the scatterers through the family of ellipsoids of constant path delay. This model also predicts a unique amplitude vs. path delay and doppler-shift relationship for scatterers that are moving with a given horizontal cross-path wind speed in each strata.

Successful tests of amplitude vs. doppler shift for this model were performed by synchronously pointing the UW and Collins antennas off the great circle and noting that the average doppler shift increased appropriately with antenna beam displacement from the great circle.

A more useful test of the model which is discussed in Section II became possible with the results of certain RAKE channel sounding experiments described by Barrow, et al., (1965) and Abraham, et al., (1967). Interpreting the RAKE data in terms of the model yielded layer heights and wind speeds that compared favorably with the weather bureau sonde data available at the nearest times and location. Since the RAKE technique achieves spacial resolution by the use of wide-band, short correlation-time sounding signals rather than by small antenna beams, several system advantages are realized. These are discussed in Section 3, together with a hybrid system which would employ a vertical fanbeam.

2. CW SOUNDING ON THE UW-COLLINS LINK

In the UW experiment, a phase-stable 960 MHz, CW signal derived from a 1 MHz standard is transmitted at 10 kw from a 28 ft. steerable paraboloid at the Collins Communication Research Facility (CCRF) near Cedar Rapids, Iowa, to the University of Wisconsin Facility (UW) near Arlington, Wisconsin (Figure 1). The signal received at UW on a 28 ft. steerable paraboloid is phase-coherently retransmitted at 810 MHz and 1 kw from the same (duplexed) antenna to CCRF. The transponded signal is received at CCRF on a separate 28 ft. paraboloid slaved to the CCRF transmitting antenna. The round-trip signal is phase compared with the signal from the original standard in a linear phase-detection system. The phase difference, due almost entirely to the propagation path, is continuously recorded on two simultaneously available ranges (17.12π and 60π radians). Each phase output automatically resets at its range limits, thereby providing linear, piece-wise continuous data over an unlimited number of cycles, (Figure 2). Residual phase noise of the closed-loop system is about 30° rms. Experimental error introduced by the antenna pointing systems is considered negligible. Antenna pattern measurements revealed a constant great-circle misalignment of approximately 0.2°. Data illustrated in Figures 3 through 9 have not been adjusted for this small error.

The signal phase behavior includes a wide range of variations (Birkemeier, et. al., 1965). Certain features are consistently noted. Phase "jumps" of up to, but not exceeding, π radians occur coincident with deep fades, indicating the interference nature of the fading phenomena. With the exception of these phase jumps and occasional periods of aircraft interference, the instantaneous phase rate never exceeds that which can be produced by tropospheric winds. When the antennas are aligned on the great-circle azimuth the phase has essentially zero average slope. Random variations over several minutes rarely exceed about 10π radians (Figure 2). When the antennas are synchronously set to positions off the great-circle azimuth, the phase accumulates continually in one direction (Figure 2). Random phase variations about the average slope also become more rapid, suggesting that the phase spectrum of the received signal is dependent on the antenna pointing angle.

The average slope of the phase-versus-time record corresponds to an average doppler shift and at a given antenna angle is clearly defined over a few minutes (Figure 2).

A series of beam-swinging experiments revealed the average doppler shift to be a systematic function of the antenna pointing angle and the direction

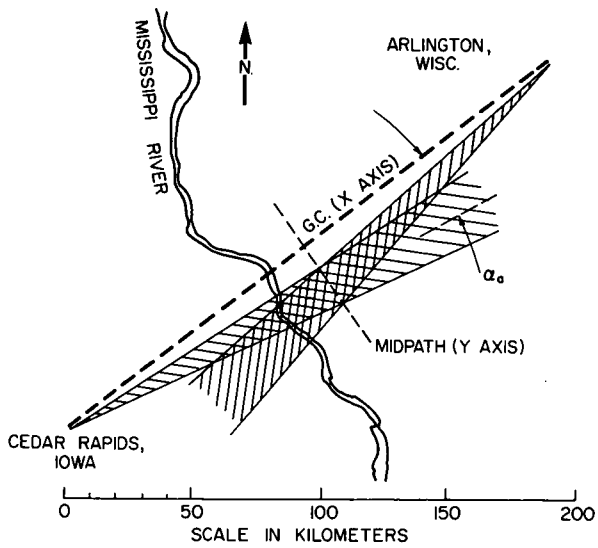

Figure 1. Plan view of closed-loop circuit illustrating geographic location, nominal antenna half-power beamwidth and azimuthal antenna-pointing angle, α_a.

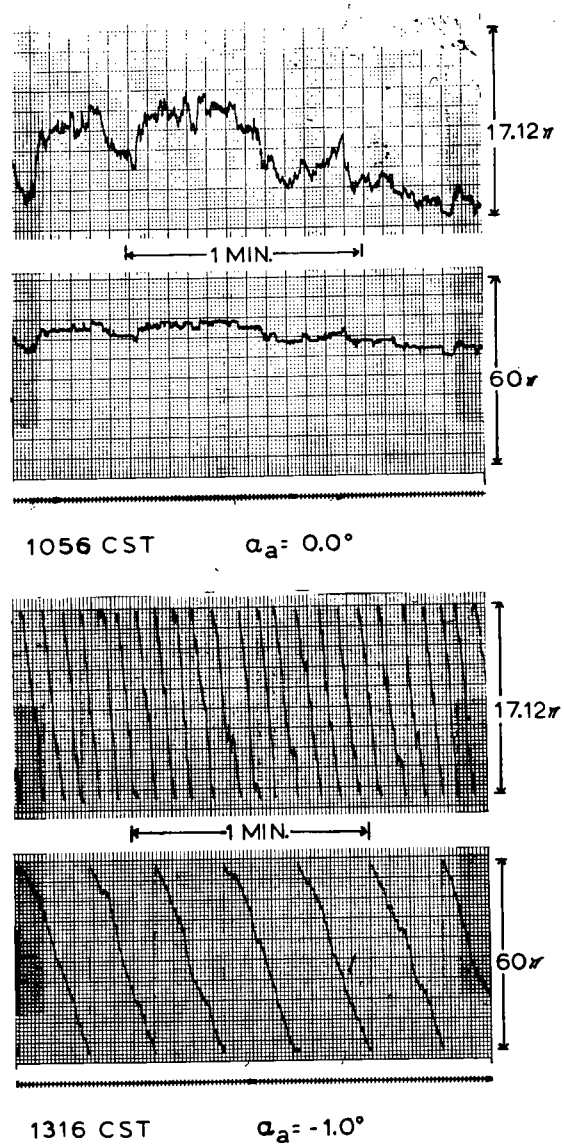

Figure 2. Typical strip-chart records of signal phase variations measured during experiment of 7 July 1966. Time markers at 1-s intervals.

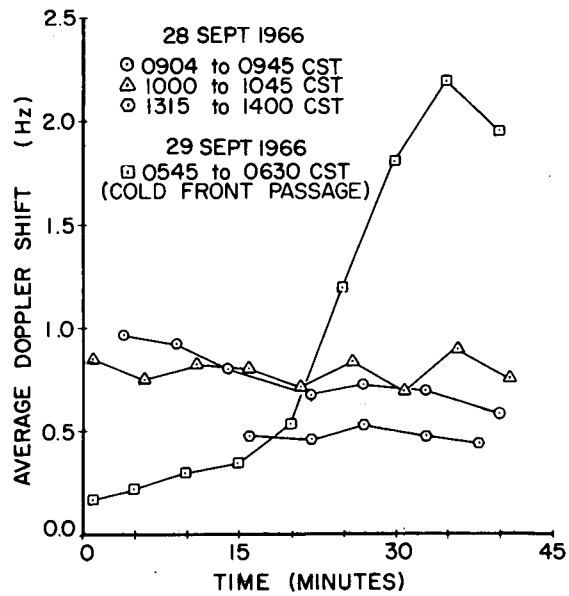

Figure 3. Measured average Doppler shifts vs. time for α_a = 1.0°.

Table 1

Beam Swinging Experiments

Experiment	Date	Time(CST)	Time at Each Angle*	Sequence of Angles**
A	10 June 1966	1437-1750	1	1
B	7 July 1966	1015-1430	2	2
C	21 Sept. 1966	1211-1313	1	3
D	28 Sept. 1966	0431-0626	3	3
E	28 Sept. 1966	1840-1915	4	3
F	29 Sept. 1966	0230-0430	3	3
G	29 Sept. 1966	1055-1145	5	4
H	24 July 1967	2225-0230	5	3
I	25 July 1967	0440-0710	6	5
J	25 July 1967	1010-1115	7	3
K	25 July 1967	1115-1200	7	3
L	25 July 1967	1200-1315	7	3

*Time at Each Angle
1. 10 minutes.
2. 15 minutes.
3. 10 minutes between 0.6° N & S, 5 minutes each larger angle.
4. 1.5 minutes.
5. 10 minutes between 0.4° N & S, 5 minutes each larger angle.
6. 4 minutes.
7. 3 minutes.

**Sequence of Angles
1. 0.2° N & S, 0.4° N & S, etc.
2. 0.4° N & S, 1.0° N & S, 1.0° N & S, 1.0° N & S, 0.6° N & S.
3. Sequentially S to N.
4. Sequentially N to S.
5. Sequentially S to N from 5.0° S, then 5.0° S to 7.0° S.

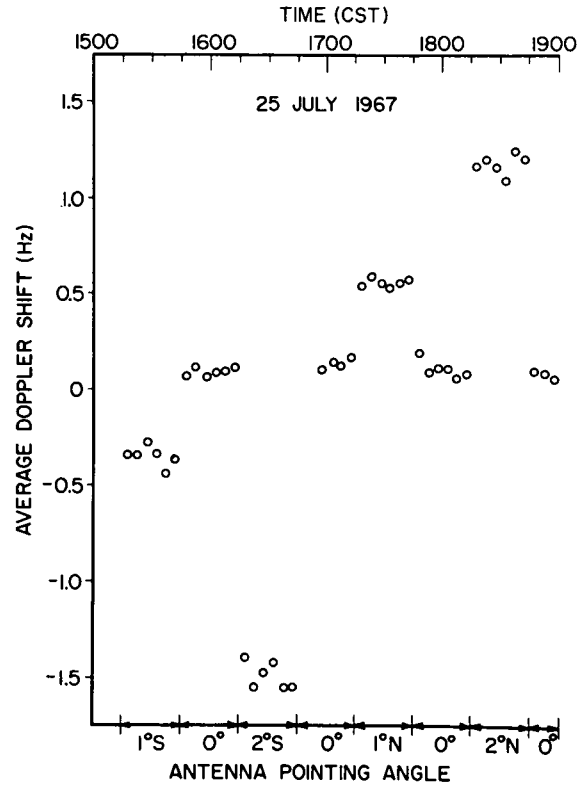

Figure 4. Measured average Doppler shifts vs. azimuthal antenna-pointing angle and time.

and magnitude of the crosspath wind. In each experiment the antennas were synchronously set for several minutes at a sequence of azimuthal angles. Experimental observations are summarized in Table 1 and Figures 5 through 9.

Doppler shifts measured at equal angles on opposite sides of the great circle are essentially identical in magnitude in Figures 5, 6 and 8. The sign of observed doppler shifts agrees with the direction of crosspath winds in the lower portion of the common volume, i.e., the received frequency is greater (less) than the transmitted when the antennas are pointed upwind (downwind). The symmetric, systematic, non-linear characteristic of these doppler shift versus antenna pointing angle curves cannot be ascribed to nonstationary meteorological processes. The daily to hourly variation in this curvature suggests dependence on the prevailing reflective angular dependence of the atmospheric refractive structure.

The observed data will be discussed in the context of the proposed doppler shift model which is developed in terms of the average crosspath wind. Concurrent wind data were obtained by tracking meteorological pilot balloons with a theodolite at launch intervals of 30 minutes to one hour. The analysis of tracking data included computation of vertical profiles of crosspath wind speed. Representative crosspath vertical profiles are shown in Figure 10. Balloons were normally launched from a field site at midpath beneath the common volume.

2.1 Doppler Shift Model

To each point in space there corresponds a ray-path length L(x,y,z) which is defined by a ray from the transmitter to receiver passing through the given

point. Surfaces of constant path length or phase are approximately ellipsoids of revolution having the radio terminals as foci (Figure 11). A signal obtained via any single moving point is shifted in frequency by an amount proportional to the rate at which the point cuts equiphase surfaces. Thus the "single-scatterer" doppler shift f is given by

$$f = -\frac{1}{\lambda}\frac{dL}{dt} = -\frac{1}{\lambda}\,V \cdot \nabla L \tag{1}$$

where λ is the wavelength and V is the velocity of the moving scatterer. Assuming the simplest ray path of two straight lines through the scatterer, L is determined using the coordinate system illustrated (Figure 11) with origin at the midpoint of the straight (chordal) line between the terminals.

$$L = [(d + x)^2 + y^2 + z^2]^{1/2} + [(d - x)^2 + y^2 + z^2]^{1/2} \tag{2}$$

Applying (1) to (2) yields

$$f = -\frac{4}{\lambda L}\,\frac{ux(1 - 4d^2/L^2) + vy + wz}{1 - 16x^2d^2/L^4} \tag{3}$$

where (u,v,w) are the (x,y,z) components of V.

The relative importance of the various terms in (3) depends on the position of the scatterer and on the relative magnitude of the velocity components. The along-path (u) contribution is negligible because the ellipsoids are longitudinally very "flat". The factor $(1 - 4d^2/L^2)$ is small, and equal to $4z_m^2/L^2 = 4h_m^2/d^2$, where z_m and h_m are the midpath heights of an ellipsoid above the chordal axis and spherical earth, respectively. This factor ranges from 10^{-4} to 10^{-2} from the bottom to the top of the common volume for the path employed in these experiments.

At a given point, the average horizontal velocity normally greatly exceeds the average vertical velocity. We interpret our observations in terms of drift of scatterers with the average crosspath velocity v. Under these conditions, (3) predicts for a single scatterer in the vicinity of midpath,

$$f = -\frac{2}{\lambda}\,v\,\left(\frac{2y}{L}\right) = -\frac{2}{\lambda}\,v \sin\alpha = -\frac{2}{\lambda}\,v\alpha \tag{4}$$

where α is the azimuthal angle of the single scatterer from the great circle. For a given crosspath wind speed, pointing the antennas to azimuthal angles away from the great circle tends to favor scatterers at larger angles α which consequently increases the observed doppler shifts. There are many scatterers at various positions, however, which create a spectrum of doppler shifts in the received signal. It is necessary to specify the doppler spectrum and its dependence upon azimuthal antenna pointing angle α_a in order to explain the shape of the curves of average doppler shift f vs. α_a.

Consider numerous scatterers moving with the wind, each contributing a signal component having a doppler shift given by (4). Because of the longitudinal flatness of the ellipsoids, scatterers even widely displaced from midpath may be included with little error. For a given constant crosspath speed the doppler shift varies linearly with crosspath position and is independent of height. The shape of the doppler spectrum which results is principally determined by the relative strengths of scattered signals as a function of crosspath position. The signal power from a given position depends upon the combined antenna illumination pattern and upon the scattering cross section at the position. Let $G(\alpha)$ denote the multiplied azimuthal pattern function of the antennas and $W(\alpha)$ the scattered power per unit azimuthal angle. For synchronously pointed antennas with boresights at α_a,

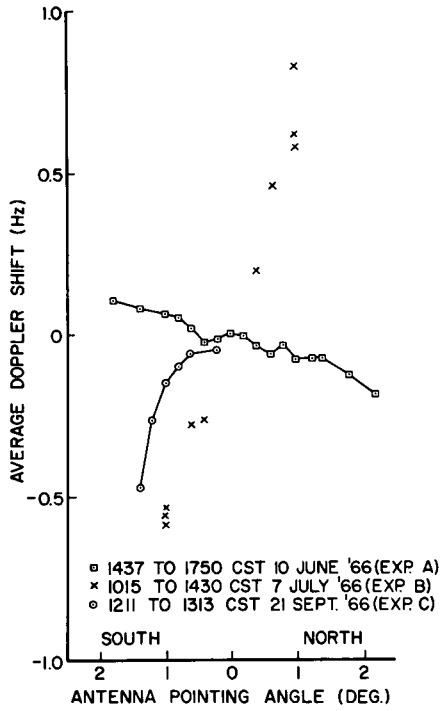

Figure 5. Measured average Doppler shifts vs. azimuthal antenna-pointing angle.

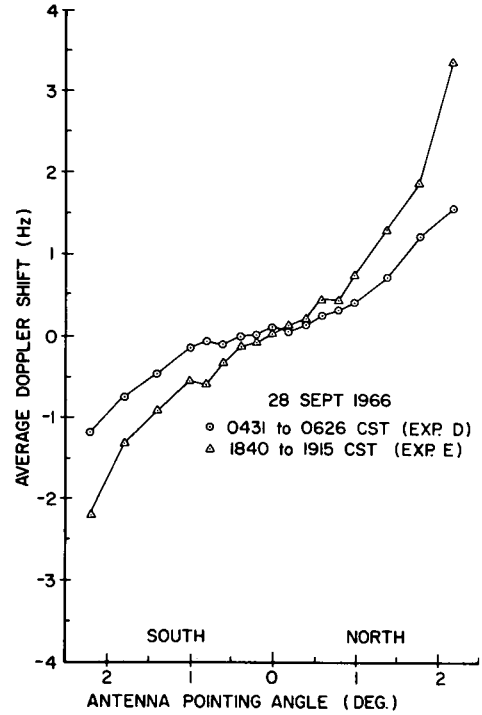

Figure 6. Measured average Doppler shifts vs. azimuthal antenna-pointing angle.

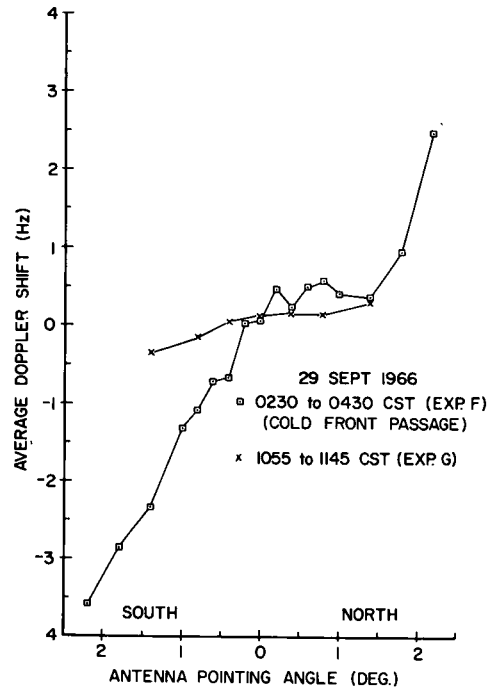

Figure 7. Measured average Doppler shifts vs. azimuthal antenna-pointing angle.

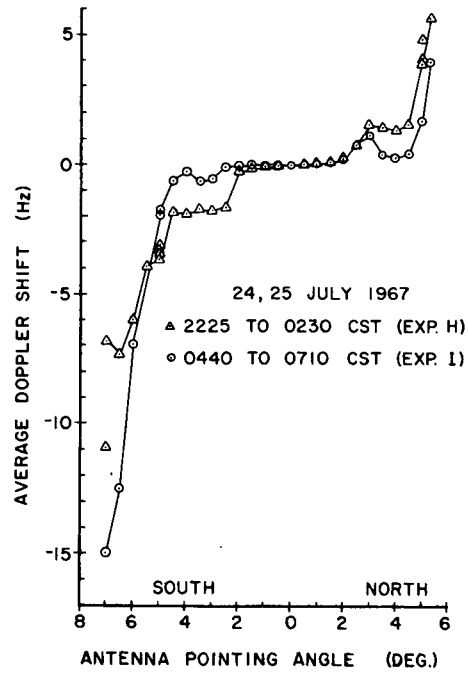

Figure 8. Measured average Doppler shifts vs. azimuthal antenna-pointing angle.

$$S(f)\ df - S_\alpha(\alpha,\alpha_a)\ d\alpha = G(\alpha-\alpha_a)\ W(\alpha)\ d\alpha \tag{5}$$

where S(f) is the doppler spectrum $S_\alpha(\alpha,\alpha_a)$ is the doppler spectrum written in terms of α, and f and α are related by the scaling relation (4).

Bello (1965) gives the average doppler shift f in terms of the doppler spectrum as

$$f = \int f\ S(f)\ df / \int S(f)\ df \tag{6}$$

which according to (4) and (5) may be written

$$f = -\frac{2v}{\lambda} \int \alpha G(\alpha-\alpha_a)\ W(\alpha)\ d\alpha / \int G(\alpha-\alpha_a)\ W(\alpha)\ d\alpha \tag{7}$$

This equation provides a relation between f and α_a in terms of the antenna patterns and the "angular dependence" function W. W includes the azimuthal dependence of scattering cross section and/or reflection coefficient depending on the degree of anisotropy of the atmospheric structure involved. W is assumed to decrease monotonically and symmetrically with increasing angle from great circle. The doppler spectrum S is weighted by W toward the great circle from α_a, and the average doppler shift is reduced from the value associated with scatterers at α_a.

An angular dependence function for reflectivity based upon the Tatarski (1961) model for a refractively turbulent medium is

$$\eta = \text{const} \quad \sin^2\beta \ / \quad \sin^{11/3}(\theta/2) \tag{11}$$

where θ is the scattering angle and β is the angle between the electric field vector and the ray to the receiver. The combined wind and phase data suggested that dominant signal contributions were frequently propagated via a low layer of limited vertical extent. Supporting observations of tropospheric layer structure by Atlas, et. al. (1966) and Hardy, et. al. (1966) using radar backscatter, and by Lane (1966) using radar and radio refractometers, stimulated analysis of a thin, turbulent scattering layer. Using η (with $\sin^2\beta = 1$) and gaussian antenna patterns, the "doppler spectra" of Figure 12 were computed from (5). The peaks of $S_\alpha(\alpha,\alpha_a)$ occur to the great-circle side of the pointing angle. These spectra are converted to doppler spectra by means of the scaling relation (4) for a given average crosspath wind velocity. Numerical integration of (7) for such doppler spectra yields the set of average doppler shift versus antenna pointing angle curves of Figure 13 for several heights of the thin, turbulent scattering layer. These curves are symmetric in α_a, a property of (7) for symmetric W and G. A change in the magnitude or direction of the crosspath wind changes the vertical scale or the sign of the curves but not the shapes. The foregoing doppler shift model provides the qualitative features and correct orders of magnitude required to interpret the data.

2.2 Interpretation

The crosspath wind profiles have in several cases permitted identification of the height range of significant scattering.

During experiments conducted on 7 July 1966, 21 September 1966, 29 September 1966 and 24, 25 July 1967, the crosspath component of the wind was from the northwest (NW) at all altitudes. The sign of the average doppler shift corresponded to this direction, i.e., was positive (frequency increase) for antennas directed toward the windward side of the great circle, and negative (frequency decrease) for the leeward side. During the experiments of 25 July 1967 in which the beams were azimuthally swung in both an unelevated and elevated position, the average doppler shift was greater for the cases of elevated beams (Figure 9). The observed increase was in agreement with greater wind speeds

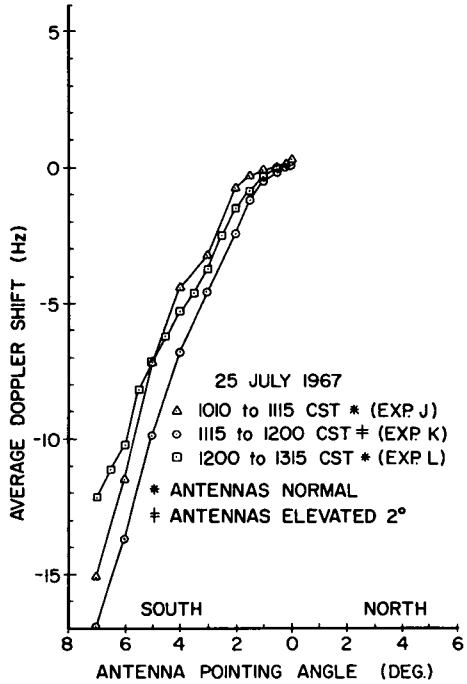

Figure 9. Measured average Doppler shifts vs. azimuthal antenna-pointing angle.

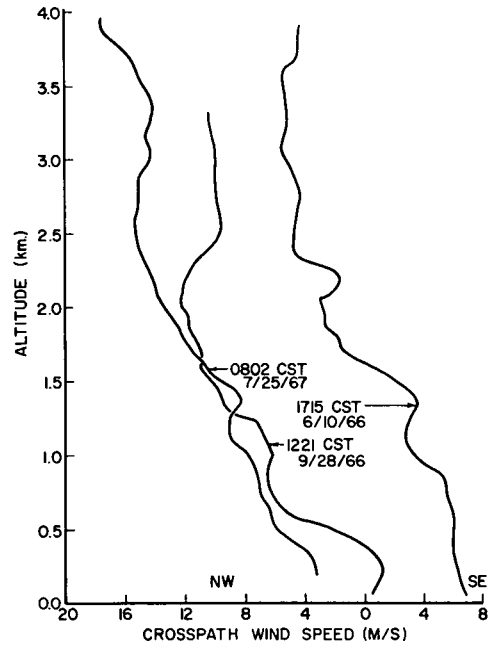

Figure 10. Typical crosspath wind profiles measured during varied meteorological conditions.

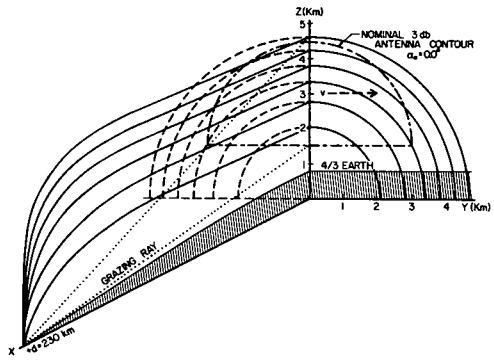

Figure 11. Longitudinal and transverse sections of propagation link and of ellipsoids of constant path length. Path length increment between ellipsoids is 80λ shown for λ = 0.37 m.

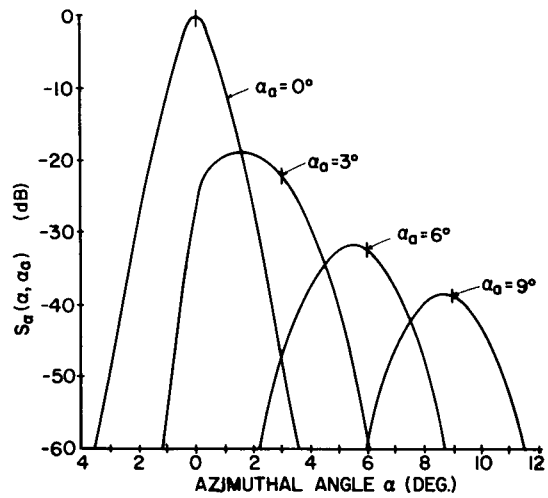

Figure 12. Theoretical Doppler spectra (written in terms of α) for different α_a for a thin, turbulent scattering layer at 785 m above the earth, computed using Tatarski scattering cross section and Gaussian antenna patterns (each with 3.0° half-power beamwidth).

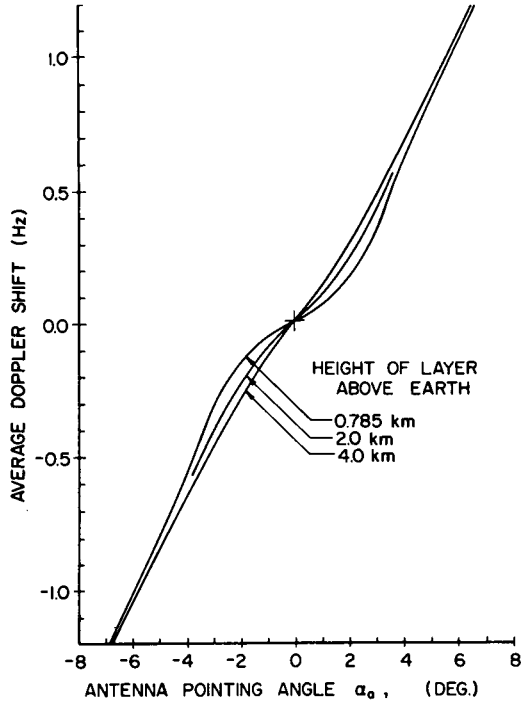

Figure 13. Theoretical average Doppler shift vs. antenna-pointing angle for the two-way path for thin, turbulent scattering layers, computed using Doppler spectra such as those of Fig. 12. Indicated heights are approximately at the bottom, middle and top of the nominal common volume, v = 1 m/s.

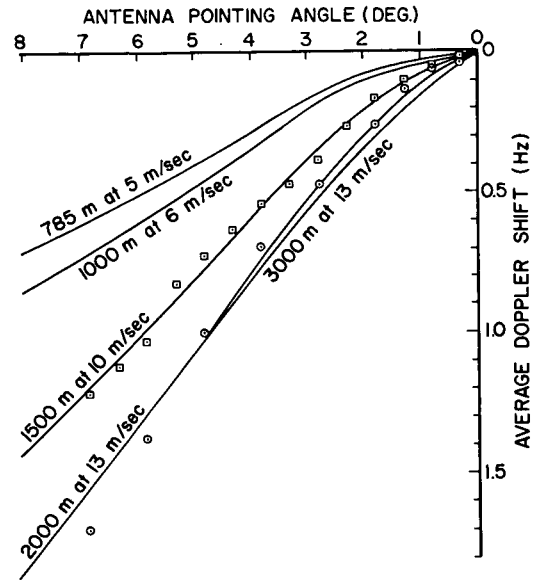

Figure 14. Comparison of data of experiments K and L (Fig. 9) with theoretical average Doppler shift for several layer heights. Wind speeds are average of those measured at the indicated heights during the experiment. Data are compensated for 0.2° constant misalignment.

measured at the higher altitudes.

Experiments on 28 September 1966 were conducted when the crosspath component was from the NW at all heights above approximately 400 m altitude but from the southeast (SE) between the surface and the reversal height (Figure 10). During the experiments the sign of the doppler shift corresponded to NW winds. Thus although a large percentage of the total propagation path is at altitudes below 400 m, this region did not appear to contribute the significant doppler-shifted signal components.

During the experiment of 10 June 1966, the crosspath component was SE below, and NW at all heights above 1.6 km. The sign of the average doppler shift corresponded to the SE winds in the lower portions of the common volume.

A vertical beam-swinging experiment in which the crosspath wind reversed direction from SW to NW at a height of approximately 1.5 km was conducted on 12 May 1967 and phase data is shown in Figure 15. With the antennas set 2.0° off the great-circle azimith and at 0.0° elevation, the sign of the average doppler shift corresponded to the SE winds in the lower zone. When the beams were elevated to 2.0°, the average doppler shift reversed to the sense corresponding to the NW winds above 1.5 km. This result suggests that a crossed pair of bistatic, doppler-sensitive systems, measuring both crosspath wind components, might be used to remotely measure winds.

In their entirety these observations demonstrate that the dominant signal contributions were reradiated in the lower regions of the common volume, as distinct from either the upper portions of the common volume or the regions between the antennas and the common volume. This interpretation agrees with the conclusions of earlier studies based on statistical analysis of amplitude data by Ikegami (1960) and Fengler (1964). The next section on the RAKE data also confirms that stronger reflecting layers tend to be the lowest in elevation.

In Figure 14, theoretical curves, similar to those of Figure 13 but computed for single layers at different heights, are compared with the data of Figure 9. For clarity, only two data curves are included. The theoretical curves are scaled for the measured winds at the labeled heights. At low altitudes, where the wind speed increased with height, the height region of agreement is well resolved. The height of agreement for the case of elevated beams is poorly defined because the wind velocity was essentially constant between 2 and 3 km altitude. Good resolution was also obtained when the same procedure was applied to the data of Figure 6. The heights of agreement were about 1.5 and 2.0 km for experiments D and E respectively.

The model based on the Tatarski hypothesis is inadequate to explain features of the data of Figure 8 which were obtained during a stable, stratified nocturnal atmosphere. Stable layers may produce highly anisotropic space correlation functions of index of refraction that yield spectral energy only at wave numbers nearly normal to the earth's surface. This results in quasi-specular components arriving only via paths near the great circle plane. For this reason these components have nearly zero doppler shift independent of their scatterer's crosspath speed. Their contribution to the doppler spectrum is accounted for by emphasizing the angular dependence function W at small α. Since many strata of scatterers with differing angular dependence functions and differing wind speeds would normally be included within the UW link's antenna beams, it is hazardous to try to associate the W function in a given experiment with a single layer. However, in the next section it will be shown that such an identification may be possible with RAKE probing even with large beams.

3. RAKE TROPOSCATTER SOUNDING

The experiments of Barrow (1965) and Abraham (1967) analyzed in this section were the first reported tests of the RAKE adaptive communication system applied to the troposcatter channel.

In its normal communicating mode of operation this system employs an estimator-correlator receiver containing a stored alphabet of reference signals. The decision as to which signal from the alphabet was transmitted in each signaling interval is determined by cross-correlating the received signal with each stored reference signal and selecting the one with the greater correlator output.

Since the received signal is distorted by the channel, the correlation process can be enhanced by predistorting the reference signals in the alphabet in an identical manner. To allow this, the receiver must learn the channel transfer characteristic and implement it as a delay-line model into which the reference signals are fed before cross-correlation with the arriving signal. It is the data from the channel sounding operation that is interpreted here in terms of the atmospheric layer structure and the crosspath winds.

To enable the RAKE receiver to learn the channel's transfer characteristic, i.e., its various paths, their delays, gains and doppler shifts, a 10 MHz wide phase-stable, periodic, pseudo-random sounding signal is transmitted continuously. Cross-correlation of this received signal with its replica at the receiver provides a correlation function which is proportional to the received signal intensity at those correlator delays which match the various path delays

of the channel. This cross-correlation function is the path-delay profile. A delay resolution of 0.1 μsec. is provided in these data. Furthermore, the doppler shift associated with each path shows up as the beat-frequency of the cross-correlator output at that path delay setting. Figure 16 from Barrow (1965) shows an example of such a cross-correlation function produced by linearly increasing the reference signal delay at the rate of .1 μsec. per second. Note the total channel path-delay profile width is about 2.8 μseconds.

A systematic increase in doppler frequency with delay is clearly visible in the profile. This was plausibly interpreted by Barrow in terms of vertical wind velocities through the common volume, with higher vertical wind speeds at higher altitudes. However, it can be shown that the profile agrees closely with the result expected from a thin layer of scatterers moving essentially only with the horizontal wind. To show this, the doppler cycles in the profile were counted, starting at the first arrival, and the resulting function compared to that predicted by the model. To get the predicted function, consider a scattering point at (y,z). The path delay at the point relative to (0,z) is given by (2) and amounts to

$$\tau = (L - L_{min}) / c = y^2 / \; c(d^2 + z^2)^{1/2} = ay^2 \tag{12}$$

Next, let the reference signal delay be varied linearly in real time t at the rate of p sec/sec. If the total number of doppler cycles appearing in the swept multipath delay profile is counted as a function of sweep time T, beginning with the first-arriving signals, the result is given by

$$N(T) = \int_0^T f_d(t)\, dt \tag{13}$$

where $f_d(t)$ is the doppler beat frequency as a function of time.

Recalling that for the model the doppler shift varies linearly with cross-path displacement y and that the delay time τ varies as the square of y, we have from (4) and the relation $\tau = pt$,

$$f_d(t) = bvy = bv(\tau/a)^{1/2} = bv(p/a)^{1/2}\, t^{1/2} \tag{14}$$

where b, v, a and p are constants.

Finally,

$$N(T) = K \int_0^T t^{1/2}\, dt = \text{const}\; T^{3/2} \tag{15}$$

Figure 17 shows a log-log plot of N vs. T using the raw, counted data of the profile. A clear power-law dependence is demonstrated, with the empirical power equal to 1.58.

Further consideration of this multipath profile revealed the likelihood that the antennas of the RAKE link were both displaced about one-half beamwidth to one side of the great-circle path. This was evidenced by the fact that, if the model is correct, the envelope of the multipath profile appears to violate the possible laws of angular dependence. The envelope peaks at about .8 μseconds and then falls with increasing delay. No AGC was used. The total envelope amplitude change is also about 6 db, similar to the combined antenna patterns, suggesting the profile is due to a horizontal scattering layer lying near the bore-site intersection of the beams. Using the known antenna elevation angle, the suspected antenna position is shown superimposed on the cross-section of the ellipsoids of constant time-delay in Figure 18.

Meanwhile, continued data analysis by the original authors developed the doppler spectra for the signals arriving at 0.1 sec. time-delay intervals. These spectra revealed a consistent negative doppler shift. See, for example, Figure 19a. The prevailing cross-path winds were determined from weather bureau data to be from the West, indicating azimuthal antenna displacement to

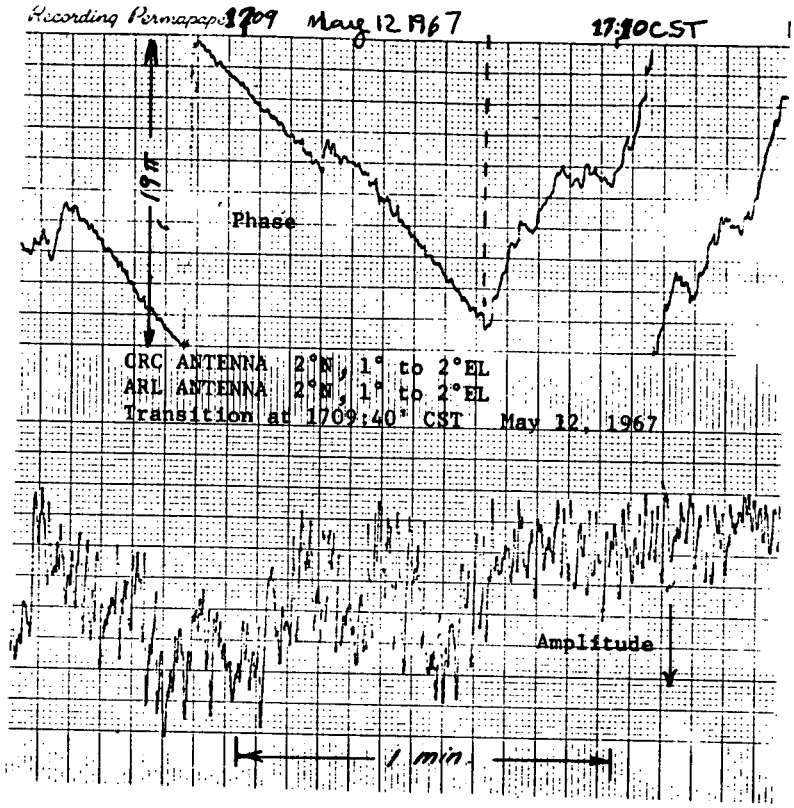

Figure 15. Doppler shift reversal with 2° antenna elevation. Clock offset was -23π rad/min.

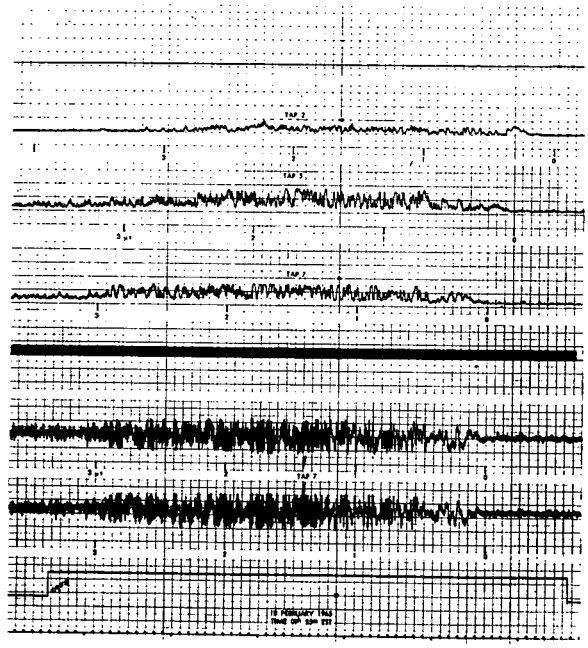

Figure 16. Quadrature components of swept multipath profile from Barrow, 1965. This profile followed scattering function 151 of Figure 19 in time by 6 hours.

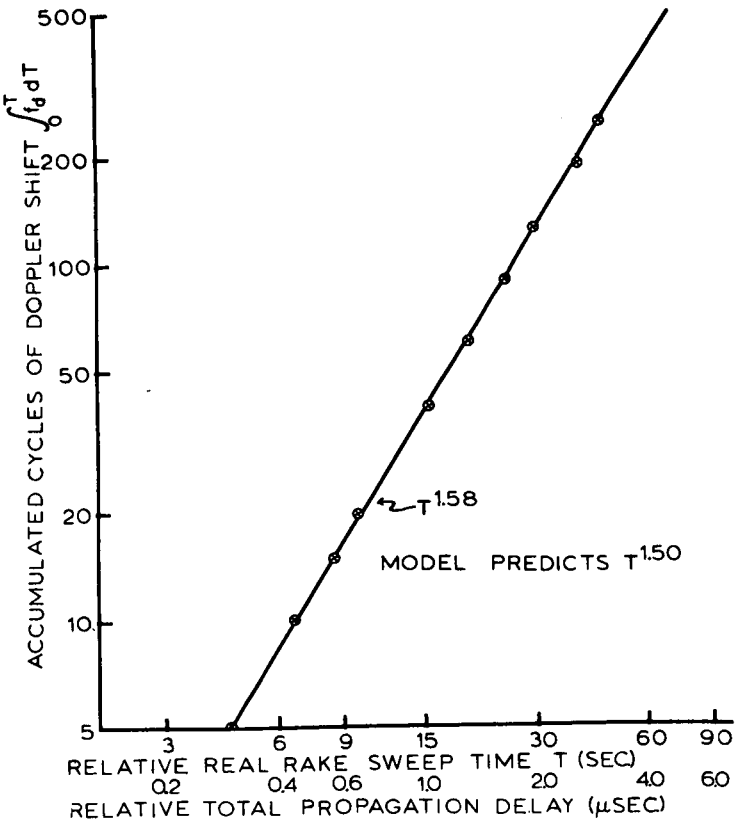

Figure 17. Plot of accumulated doppler-beat cycles vs. sweep time.

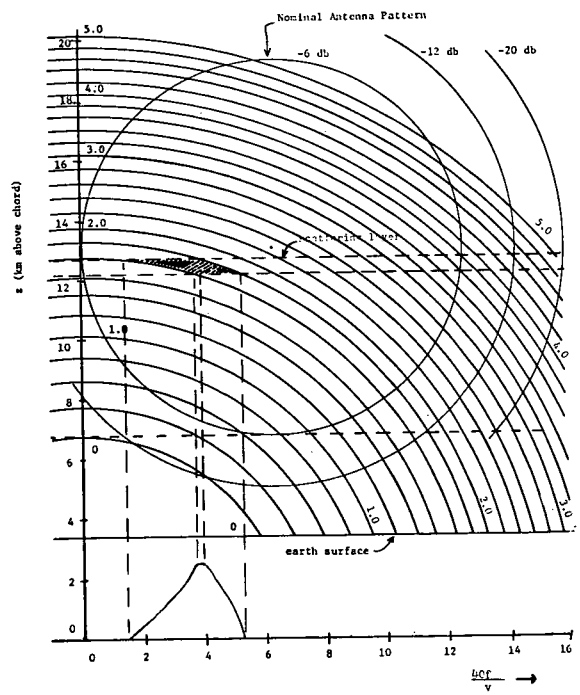

Figure 18. Apparent antenna position for RAKE link. Also shown is the construction of a doppler-spectrum from a single 0.1μ sec time shell and a single scattering layer.

the East of the path. This predicted antenna displacement was consequently investigated by the original authors and the displacement to the East has been confirmed. The exact position is not known to this writer, however.

3.1 Atmospheric Structure From RAKE Profiles

In each of the RAKE scattering diagrams (Figures 19a, 23, 25) ridges of peaked doppler-spectra appear to follow parabolic loci in the time-frequency plane. Such loci are predicted by the model for each scattering strata by the fact that horizontally drifting scatterers increase their doppler shift linearly with y while their signal delay increases with y^2. Combining (12) with (4) and using the dimensions of the 480 km RAKE path, we obtain the delay-doppler locus for point scatterers at a height z and moving with cross-path wind speed v as

$$\tau = 21.8\ f^2/\ v^2 + z^2/72 - .64 \qquad (16)$$

Here τ is in microseconds relative to the ellipsoidal shell at the grazing ray intersection which represents the scattering location of the first possible arriving signals; f is in Hz, v is in meters/second, and z is in kilometers above the link chord.

To facilitate the interpretation of the RAKE profiles in terms of the implied layer structure, a program was written on the basis of the model to determine the theoretical ridge for an arbitrary layer height, thickness, and cross-path wind speed and angular dependence function. In this program the relative doppler power spectral density for a given delay shell is proportional to the vertical thickness of the scattering layer in the shell at a particular value of y (or f), multiplied by the displaced antenna function and the angular dependence. Figure 18 shows the sketch of the spectrum obtained from a single shell. A theoretical ridge is shown in Figure 20 for a layer with Tatarski angular dependence, a height of 12.8 km, a thickness of 0.4 km, and a cross-path windspeed of 45 m/second. These values produce good agreement to the dominent ridge in the RAKE scattering function in Figure 19a. The spectrum at the origin in the RAKE diagram is assumed to have originated from signals scattered from near the great-circle plane at the grazing ray height. This determines the reference delay for each higher layer.

A number of additional parabolic tracks in this profile have been identified by plotting local spectra maxima for each shell. (See Figure 19b). Furthermore, several sharp spikes along the zero-doppler shift axis imply the existence of several specular layers as well. In an effort to compare these "radio identified" layers with the atmospheric structure in the vicinity of the link we resorted to the nearest weather bureau radio sonde profiles of wind, temperature, and humidity for the dates of the RAKE tests. Analysis of these data led to a set of probable layer heights together with their respective cross-path wind speeds. Using (16) each meteorologically identified layer's parabolic track was plotted and compared with the radio-deduced layer heights and winds. Figure 21 shows surprising agreement with the radio-detected layers since the sonde data precedes the radio run by eight hours. The result is nevertheless intriguing. Figure 22 based on the same profile shows the radio layers drawn in cross section across the antenna pattern. Wind profiles from the three weather stations are included for comparison to the radio-derived wind in each layer. The dashed lines indicate radio layers for which only the zero-doppler shift point on its track could be identified. The fact that such layers are likely to be specular agrees with the stable state of the atmosphere at their location as indicated by the sonde data.

In Figure 24 the radio layers corresponding to the parabolic tracks of the scattering function of Figure 23 are shown. It is apparent that the first 0.8

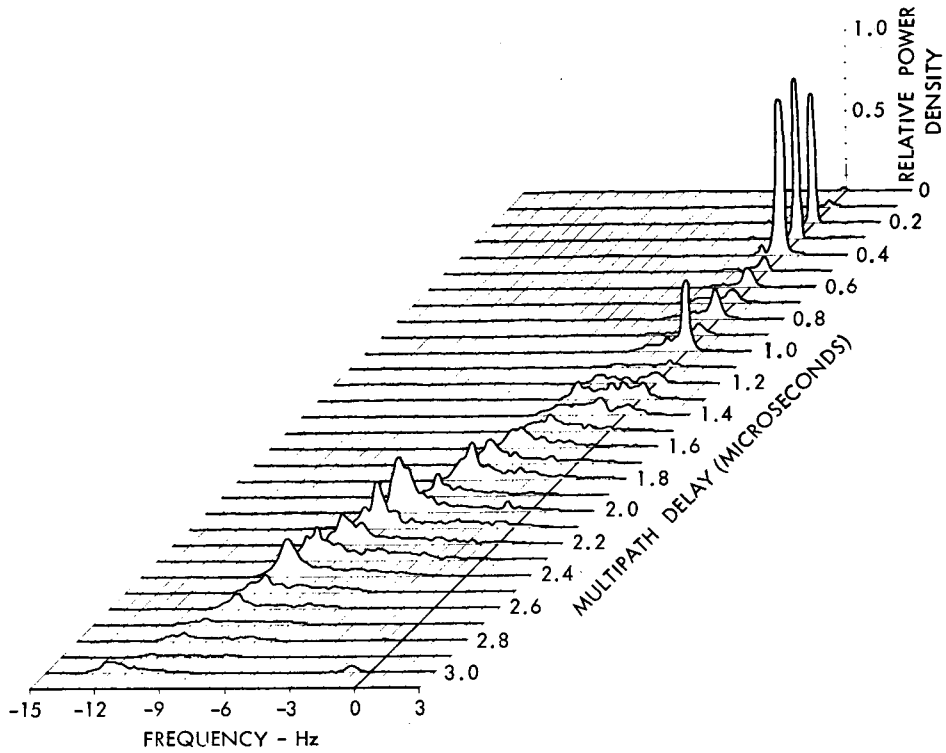

Scattering Function, Record No. 151

Figure 19a. Scattering diagram No. 151 (Abraham, 1967). Test data 2/18/65, 0821 GMT.

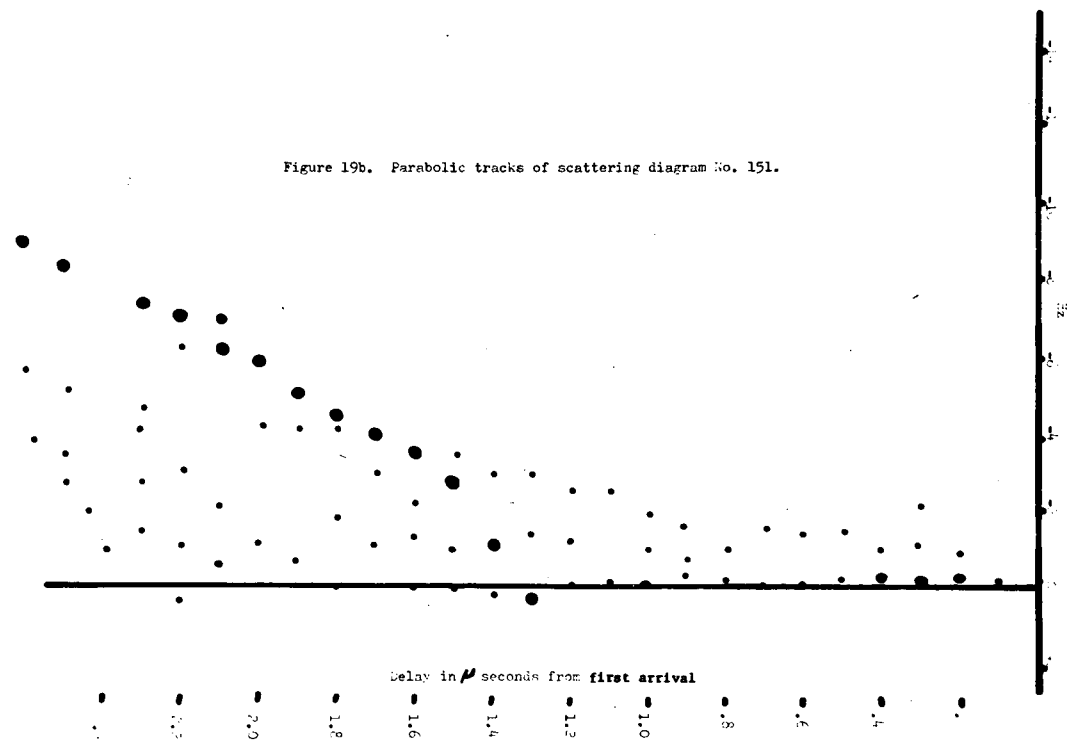

Figure 19b. Parabolic tracks of scattering diagram No. 151.

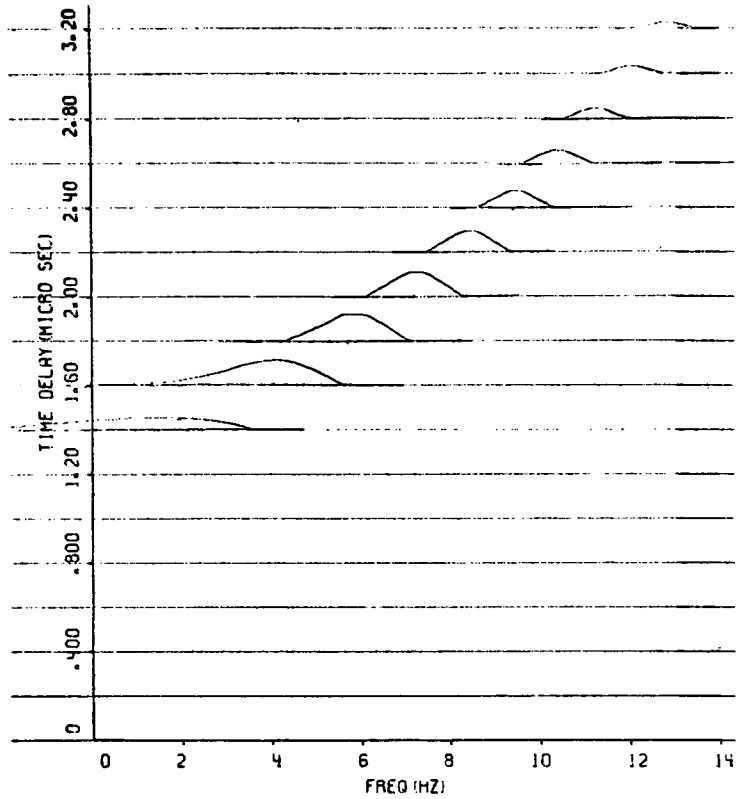

Figure 20. Theoretical scattering diagram for a layer of thickness = 0.4 km, height above chord = 12.5 km, and cross-path wind speed = 45 m/s.

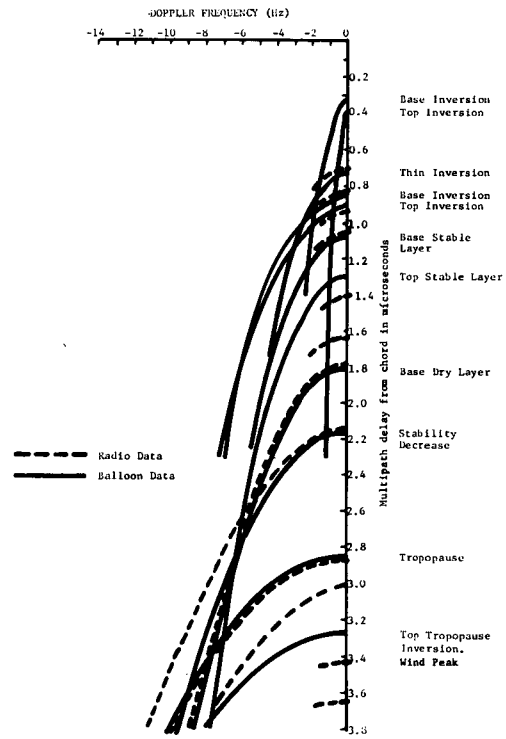

Figure 21. Comparison of RAKE parabolic tracks with tracks derived from meterological sounding. Washington, D. C. sonde preceeded radio run No. 151 by 8 hours.

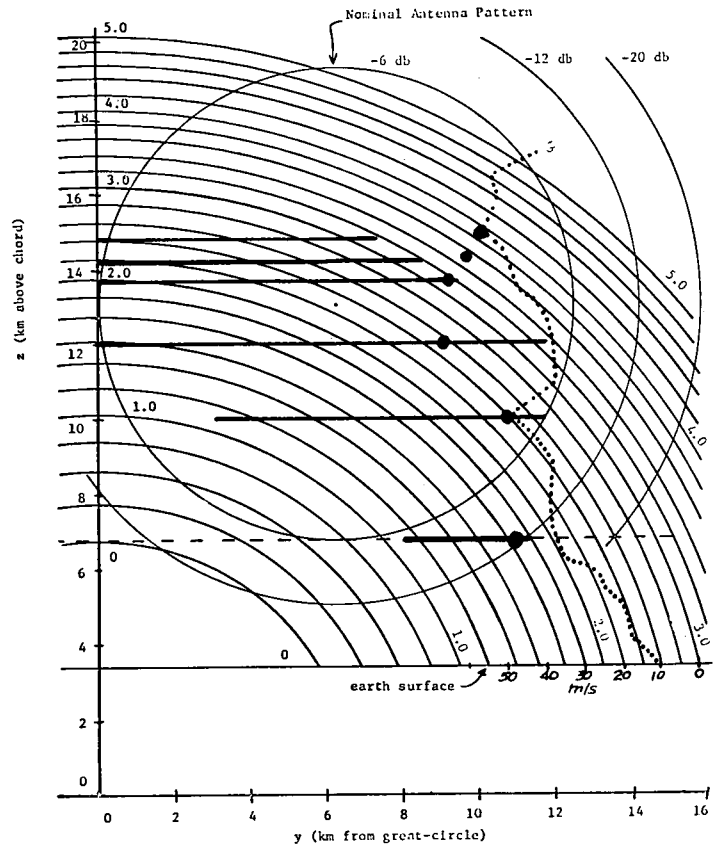

Figure 22. Atmospheric cross-section derived from Figure 19 (Scattering-function 151). Radio-derived wind-speed shown by large dots. Radio data 2/18/65 0821 GMT, Sonde data 3/18/65 0000 GMT.

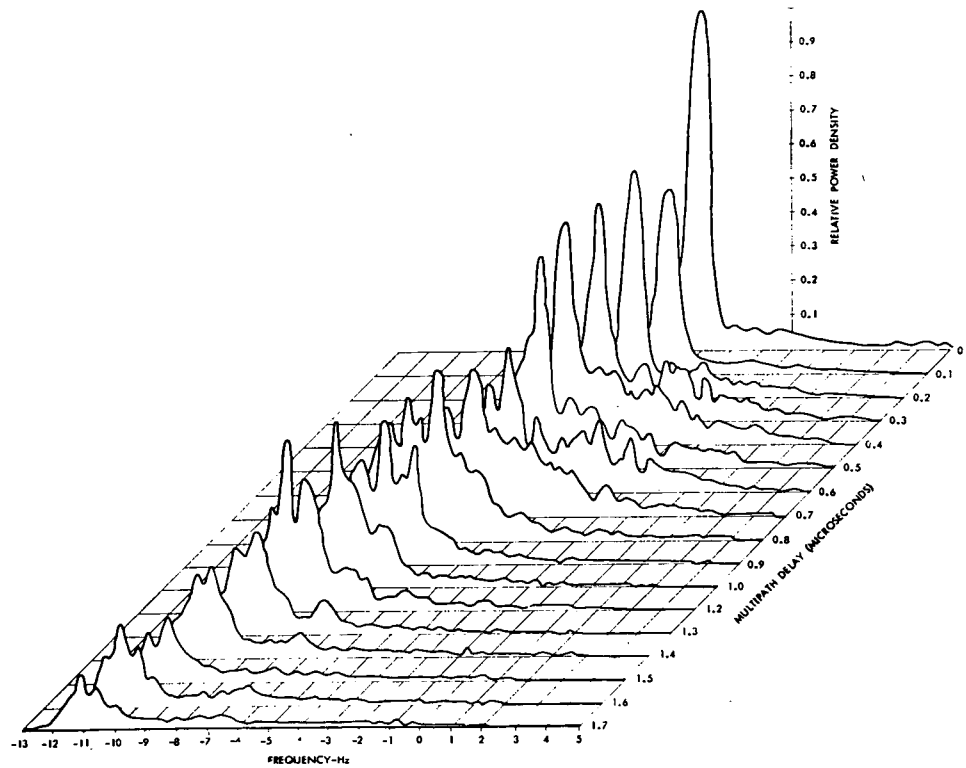

Figure 23. Scattering diagram No. 134 (Abraham, 1967).

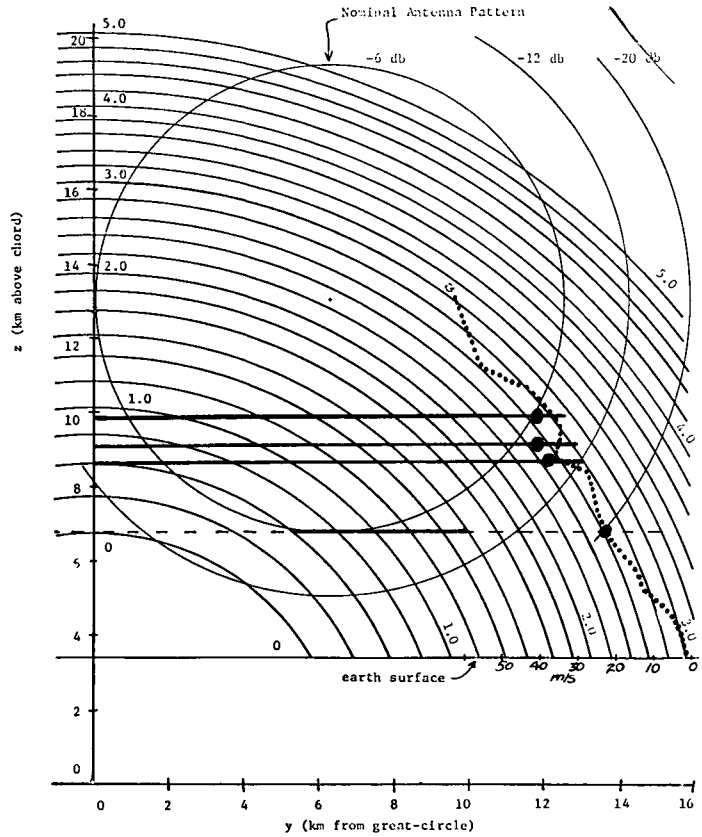

Figure 24. Atmospheric cross-section derived from Figure 23 (Scattering diagram 134). Radio data 2/17/65 2226 GMT, Sonde data 2/18/65

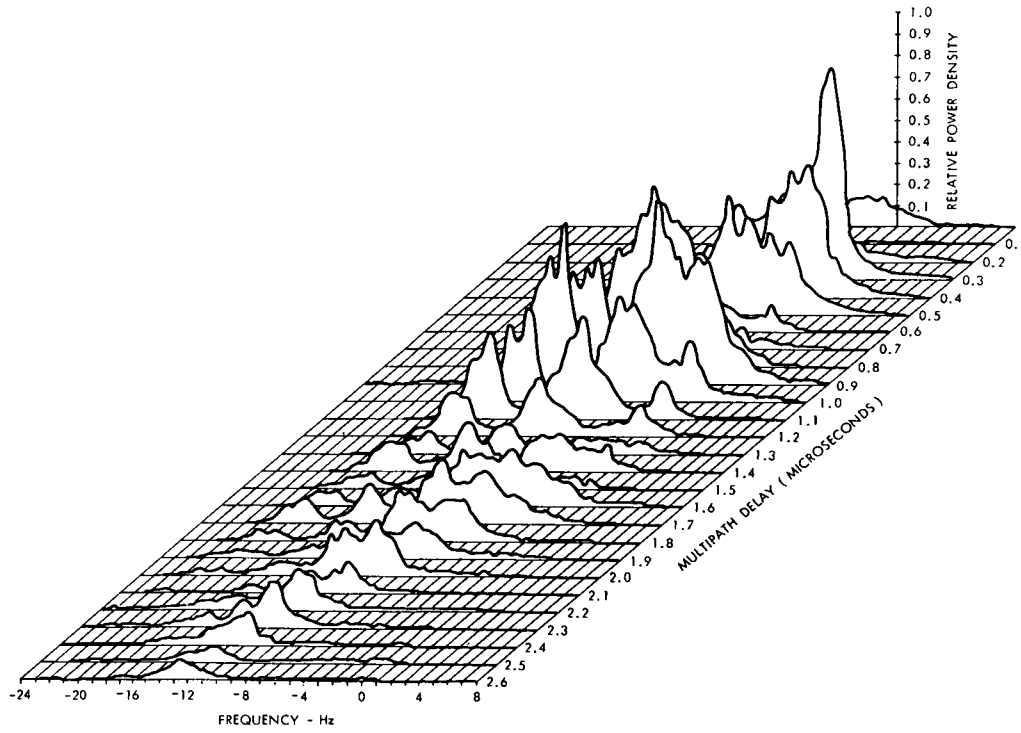

Figure 25. Scattering diagram No. 181 (Abraham, 1967).

microseconds are not included in the display. As such, the solid line segments indicate that part of the layer which contributed to the segment of the ridge in the scattering function.

The scattering function of Figure 25 appears to have coincided with a frontal passage. The cross-section derived is shown in Figure 26.

3.2 Considerations of Angular Dependence

Most of the parabolic ridges analyzed so far show general agreement with the -11/3 power law. It is difficult to determine the power law exactly, however, since neither the antenna pattern nor its position is known accurately. Further RAKE studies performed carefully, however, may well allow the angular dependence to be determined for particular turbulent layers.

In certain RAKE data, strong angular dependence is implied by "spikes" along the zero-doppler shift axis in the RAKE scattering functions. An example is the scattering function shown in Figure 27. The analysis of this and similar profiles is in progress to evaluate the exact angular dependence function and, if possible, the degree of anisotropy of the space correlation function of the index of refraction in the layer.

3.3 Tilted Layers

Under certain atmospheric conditions, scattering layers may be uniformly slanted with respect to the horizon or layers may contain uniformly slanted "scatterers". If such scattering surfaces are visualized against the background of the ellipsoids of constant phase of path delay, it is apparent that maximum reflectivity will tend to occur off the great-circle at the point of greatest tangency of the scattering surfaces to the ellipsoids. A RAKE parabolic profile for such a layer (for antennas aimed along the great circle) should then peak to the side of the zero-doppler axis, indicating "slanted anisotropy" in the space correlation function of the refractive structure. There is the possibility that the antennas of the RAKE link were aligned under such a slanted atmospheric structure, accounting for their fixed misalignment.

4. PROPOSED HYBRID SYSTEMS

4.1 Measurement of Vertical Wind Velocities

An important limitation of the simplified model presented here, in spite of the apparent agreement with this particular RAKE data, is that it ignores turbulent velocity fluctuations in the wind. Such random variations in velocity become quite important if the cross-path wind component is small compared with the total wind speed. The effect of the velocity fluctuations is to spread the doppler spectra at the various RAKE delays. This greatly complicates the problem of calculating layer thickness from the RAKE data. A Scheme to measure the vertical velocity fluctuations by eliminating doppler shift due to horizontal motion is suggested by the link geometry. Both spatial resolution from the beams and time resolution from the RAKE are required. If the antennas are designed to produce vertical fan-beams sufficiently narrow to illuminate only the first Fresnel zone along the great-circle plane, then according to (3), doppler shift can occur only from vertical scatterer motion. (Tests with beams of 0.3° width will be attempted on the UW-Collins link in the near future) Combining such fan-beams with a RAKE system to provide height resolution should allow doppler-sensing of the vertical wind velocity field. Horizontal turbulent velocities may be measured similarly by azimuthally displacing the beams off the great circle, correcting for the vertical velocity fluctuations in the measured doppler shift fluctuations.

4.2 Total Wind Measurement by Crossed Links

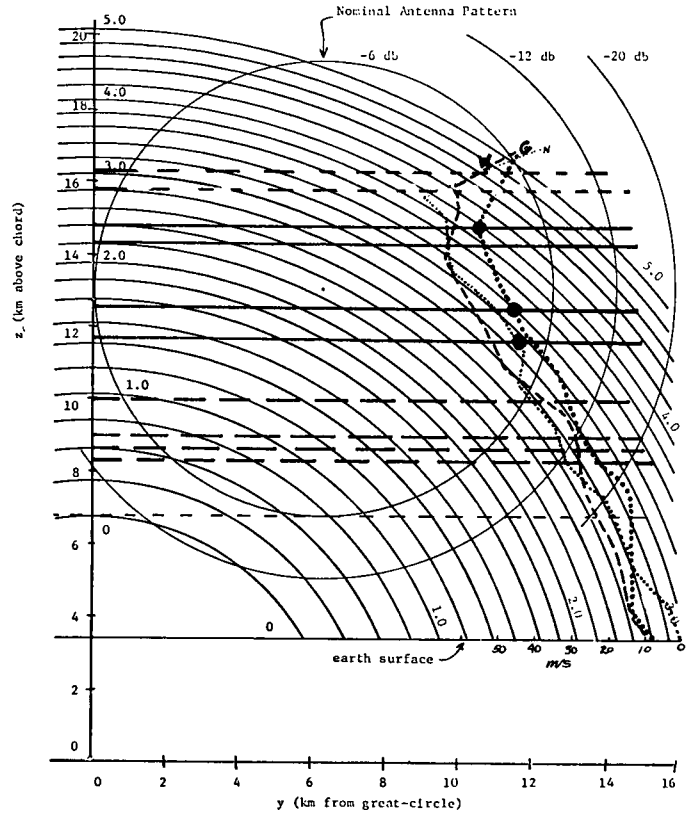

Figure 26. Atmospheric cross-section derived from Figure 25. (Scattering diagram 181). Radio data 2/19/65, 1831 GMT, Sonde data 2/19/65, 1200 GMT.

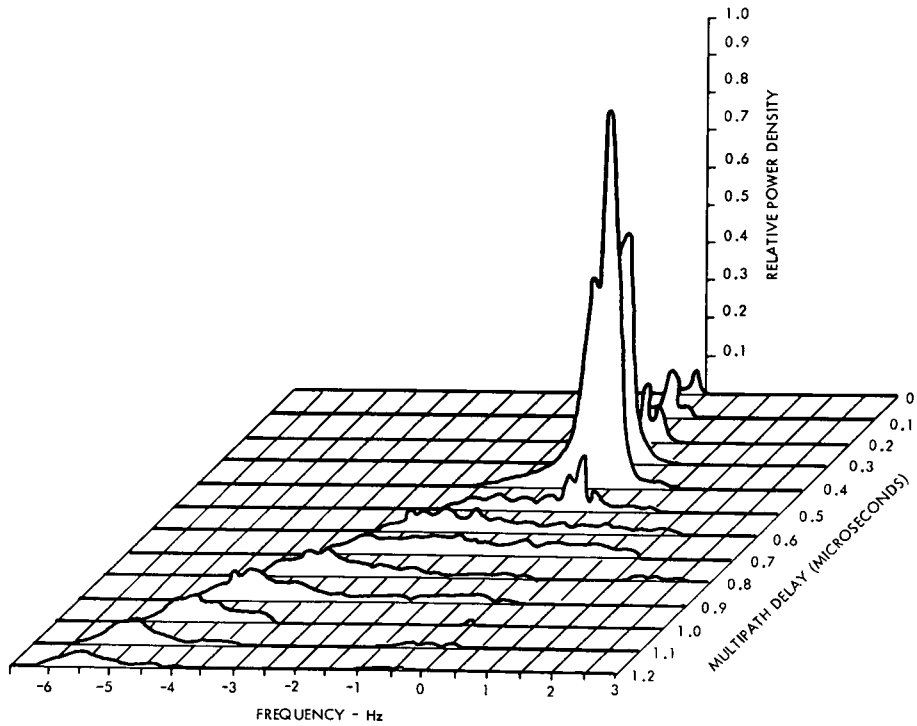

Figure 27. Scattering diagram No. 142 showing layer with strong angular dependence.

If two scatter links are arranged in parallel and spaced so that their ellipsoids of constant phase intersect orthogonally at approximately the height of the grazing ray intersection, it appears possible to measure the vertical and horizontal wind velocities simultaneously at a common point midway between the paths. This measurement is accomplished simply by forming the sum and difference of the phase outputs of the two links operating coherently on carrier-wave signals. Vertical profiles would be achieved by vertical beam swinging.

5. CONCLUSIONS

Forward-scatter atmospheric probing has been demonstrated to be potentially capable of providing useful structural information on the atmosphere. Much work needs to be done, but the combination of forward scatter's great sensitivity and the possibility of achieving spatial resolution through the use of signal processing techniques rather than by the use of large antennas makes the possibilities exciting indeed.

ACKNOWLEDGEMENTS:

Section I is taken in part from a paper entitled "Observation of wind produced Doppler shifts in troposcatter" by Birkemeier, et. al. published in April, 1968 by Radio Science.

The author is indebted to the following persons for their able assistance: D. S. Sargeant, H. S. Merrill, A. B. Fontaine, D. Atlas, D. W. Thomson, G. T. Bergemann, C. M. Beamer, and I. H. Gerks. He also wishes to thank Dr. B. B. Barrow for his interest and cooperation in supplying the RAKE data which permitted this analysis.

The work was supported by the National Science Foundation, Atmospheric Science Division, under grants GP 667, GP 4352, and GA 1291, The Wisconsin Alumni Research Foundation, and the Collins Radio Company.

REFERENCES

Abraham, L. G., B. B. Barrow, W. M. Cowan, and R. M. Gallant, May, 1967: "Tropospheric Scatter Multipath Tests in the Caribbean," Sylvania Electronic Systems, Applied Research Laboratory, Waltham, Massachusetts.

Atlas, D., K. R. Hardy and T. G. Konra, 1966: Radar Detection of the tropopause and clear air turbulence, Proc. XII Weather Radar Conf., 17-20 October 1966, Norman, Oklahoma.

Barrow, B. B., L. Abraham, S. Stein and D. Bitzer, 16 April 1965: "Tropospheric-Scatter Propagation Tests Using a Rake Receiver," 1st Annual IEEE Communication Convention, Boulder, Colorado, June 7-9, 1965. Also available as Research Report 461, Applied Research Laboratory, Sylvania Electronic Systems, Waltham, Massachusetts.

Barrow, B. B., L. Abraham, S. Stein and D. Bitzer, June 1965: "Preliminary Report on Tropospheric-scatter Propagation Tests Using a Rake Receiver," Proc. IEEE, vol. 53, no. 6, pp. 649-651.

Bello, P., 1965: Some techniques for the instantaneous real-time measurement of multipath and doppler spread, IEEE Trans. COM-13, No. 3, 285-292.

Birkemeier, W. P., H. S. Merrill, Jr., D. H. Sargeant, D. W. Thomson, C. M. Beamer, G. T. Bergemann, April, 1968: "Observation of Wind-Produced Doppler Shifts in Tropospheric Scatter Propagation," Radio Science, vol. 3, No. 4, pp. 309-317.

Birkemeier, W. P., D. H. Sargeant, J. P. Aasterud, H.S. Merrill, Jr., D.W. Thomson, I. H. Gerks, C. M. Beamer and G. T. Bergemann, 1965: A Study of the lower atmosphere using scattering of microwaves, Tech. Rep. 2, Depts. of Meteor. and Elect. Engr., Univ. of Wisc., Madison, Wisconsin.

Bitzer, D. R., D. A. Chesler, R. Ivers and S. Stein, August 1966: "A Rake System for Tropospheric-scatter," IEEE Trans. on Comm. Tech., vol. COM-14, no. 4, pp. 499-506.

Crawford, A. B., A. B. Hogg and W. H. Kummer, 1959: Studies in tropospheric propagation beyond the horizon, Bell Systems Tech. J., 38, 1067-1178.

Du Castel, F. 1966: Tropospheric Radiowave Propagation Beyond the Horizon, Pergamon Press Ltd., Oxford, England.

Fengler, G., 1964: Dependence of 500 Mc/s field strength values and fading frequencies on meteorological parameters, Proc. World Conf. on Radiometeorological parameters, 14-18 September 1964, Boulder, Colorado.

Gjessing, D. T., 1964: An experimental study of the variations of the tropospheric scattering cross-section and air velocity with position in space, IEEE Trans., AP-12(1), 65-73.

Hardy, K. R., D. Atlas and K. M. Glover, 1966: Multiwavelength backscatter from the clear atmosphere, J. Geophys, Res., 71, No. 6, 1537-1552.

Ikegami, F., 1960: A preliminary study of radiometeorological effects on beyond-horizon propagation, J. R. NBS 64D (Radio Prop.), No. 3, 239-246.

Koono, T., M. Hirai, R. Inoue and Y. Ishizawa, 1962: Antenna-beam deflection loss and signal amplitude correlation in angle-diversity reception in UHF beyond-horizon communication, J. Radio Res. Lab. 9, No. 41, 21-49.

Laaspere, T., 1958: An analysis and re-evaluation of the role of horizontal drift in producing fading in tropospheric scatter propagation, Res. Rep. EEE-380, Cornell Univ., Ithaca, New York.

Lane, J. A., 1966: Experimental investigations of refractive-index variations in the troposphere, XV General Assembly URSI, 5-15, Sept. 1966, Munich, Germany (Proc. to be published).

Stein, S., 1966: in Schwarz, M., Bennett, W. R., and Stein, S. (1966), Communications Systems and Techniques, p. 360 (McGraw-Hill Book Company, Inc. New York, New York).

Strohbehn, J. W. 1963: Transhorizon-propagation measurements and simulated angular response patterns, Res. Pre., SEL-63-083, Stanford Elect. Lab., Stanford, California.

Tatarski, V. I., 1961: Wave Propagation in a Turbulent Medium McGraw-Hill Book Co., New York, New York.